RSC Advances

PAPER

View Article Online
View Journal | View Issue



Cite this: *RSC Adv.*, 2025, **15**, 50428

# Bleeding inhibiting, highly absorbent 3D-printed curdlan-based dressing insert for medical applications

Aleksandra Nurzynska, *[a] Julia Higuchi,[b] Łukasz Szajnecki,[c] Karolina Mlynarczyk,[c] Beata Podkoscielna,[c] Anna Michalicha,[a] Sylwia Terpilowska[d] and Grazyna Ginalska[e]

Received 8th September 2025
Accepted 1st December 2025

DOI: 10.1039/d5ra06767g

rsc.li/rsc-advances

Exudative wounds pose a significant challenge in clinical practice, as excessive exudate can delay the healing process and increase the risk of infection. In response to the demand for advanced dressings that not only effectively absorb excess exudate but also actively support tissue regeneration, innovative biocompatible biomaterials have been developed using 3D printing technology. Thanks to the developed synthesis method, the curdlan-based materials were enriched with calcium ions and engineered to possess a porous structure, high hydrophilicity, and significant fluid absorption capacity. A notable advantage of the proposed dressing inserts is their compact dry form, which makes them easy to handle and integrate into multilayer wound dressing systems. Despite their small size, the materials can absorb substantial amounts of fluid, making them particularly promising for the treatment of highly exuding wounds, such as venous leg ulcers. Comprehensive analyses confirmed their thermal stability, biological safety (non-toxic, non-mutagenic, and hemocompatible), and the ability to stimulate skin cell proliferation. The obtained results highlight the strong potential of these biomaterials as next-generation dressing inserts for effective management of hard-to-heal wounds.



## 1 Introduction

The incidence of hard-to-heal wounds is predominantly correlated with the presence of chronic diseases, the prevalence of which continues to escalate. Among the most prevalent types of chronic wounds are decubitus ulcers, venous leg ulcers, and diabetic foot ulcers.[1] These wounds pose a serious threat to both the physical and mental health of patients, also representing a significant economic burden worldwide. It is estimated that the costs of treating chronic wounds account for up to 6% of total healthcare expenditures in developed countries.[2] Chronic wounds vary in etiology, pathogenesis, localization, and size, posing a challenge in devising a universal treatment approach.[3] Microcirculation disorders, the presence of inflammatory states, oxidative stress, imbalance in cellular regulation, and excessive exudate contribute to the impairment of the tissue regeneration process.[4] Exudate is a significant element in the wound healing process, but chronic exudate is perceived as highly detrimental to the regeneration process. It is characterized by an increased level of matrix metalloproteinases (MMPs), excess PMN elastase, and a high concentration of reactive oxygen species (ROS).[5] It damages the surrounding tissues and increases the likelihood of bacterial colonization. Therefore, in the case of such wounds, selecting an appropriate type of dressing material is essential for the reduction of inflammatory mediators.[5,6] In recent years, numerous types of wound dressings have been developed, including, among others, gauzes, foams, films, hydrogels, hydrocolloids, alginates, gelling fibers, and superabsorbent dressings.[7] In the aforementioned chronic wounds characterized by excessive exudate, it is crucial to adjust moisture balance. Dressings that maintain a balance between the amount of excess wound exudate and the amount of exudate absorbed would be ideal.[8] Such dressings, in addition to absorbing excess exudate, should provide a moist environment, facilitate tissue repair, and support the regeneration process.[9]

Innovative and groundbreaking technological discoveries in biomedical engineering, such as 3D printing, overcome the limitations of traditional dressings that fail to meet the requirements of ideal treatment.[10] Several 3D printing techniques, including stereolithography, inkjet-based systems, and extrusion-based systems, are successfully employed in biomaterials for wound treatment. Regardless of the technique used,

[a]*Chair and Department of Biochemistry and Biotechnology, Medical University of Lublin, Chodzki 1, 20-093 Lublin, Poland. E-mail: aleksandra.nurzynska@umlub.edu.pl*

[b]*Laboratory of Nanostructures, Institute of High Pressure Physics, Polish Academy of Sciences, Sokolowska 29/37 Street, 01-142 Warsaw, Poland*

[c]*Faculty of Chemistry, Institute of Chemical Sciences, Department of Polymer Chemistry, Maria Curie-Sklodowska University, M. Curie-Sklodowska Sq. 2, 20-031 Lublin, Poland*

[d]*Department of Surgical Medicine with the Laboratory of Medical Genetics, Collegium Medicum Jan Kochanowski University of Kielce, IX Wiekow Kielc 19A, 25-317 Kielce, Poland*

[e]*Faculty of Health Sciences, Vincent Pol University Choiny 2, 20-816 Lublin, Poland*

constructs produced exhibit significant advantages over traditional dressings.[11] 3D printing technology enables the fabrication of complex structures through the appropriate bioink or filament composition.[12] The ingredients of bioinks may include natural polymers such as alginate, collagen, chitosan, and hyaluronic acid, or synthetic polymers such as polycarbonates, polylactic acid, and polyglycolic acid.[13] 3D printing technology enables the production of personalized, patient-specific microstructures with the desired size and geometry, exhibiting superior physical, mechanical, and biological properties compared to traditional dressings. Furthermore, full-process automation enhances the reproducibility of the manufactured materials and is more cost-effective than traditional synthesis methods.[10,14]

In this research, three polymers were employed to produce a bioink: (1) a natural biopolymer – curdlan, belonging to the group of β-1,3 glucans enriched with calcium ions (according to the procedure described previously;[15] (2) a superabsorbent based on the copolymer of sodium acrylate with acrylic acid; and (3) polyvinylpyrrolidone. As a result, a homogeneous biomaterial was produced, wherein each component exhibited distinct properties: curdlan with $Ca^{2+}$ supported cellular processes, the superabsorbent exhibited significant absorbent properties, and PVP served as a plasticizer. In a previous study, we demonstrated that a curdlan-based hydrogel enriched with calcium ions stimulates the viability and proliferation of normal skin cells.[15] However, this biomaterial exhibited limited absorbent properties. The current study aimed to develop a curdlan-based biomaterial with significantly enhanced absorbent characteristics while preserving favorable biological properties. The increased absorbent properties were achieved through the combination of curdlan enriched with calcium ions and a superabsorbent-copolymer of sodium acrylate with acrylic acid. This polymer exhibits the ability to absorb aqueous solutions in quantities thousands of times greater than its initial mass, while also retaining the absorbed fluid within its structure even when subjected to external pressure.[16,17] It is widely used in different industries such as cosmetics, environmental protection, toys, and hygiene products for children, as well as in the food industry, approved by the FDA as a food additive.[18] It is currently being increasingly utilized in the medical sector. Dressings based solely on superabsorbent polymers provide only exudate absorption, which is insufficient to accelerate the healing process of chronic wounds and provide relief to patients. Wang *et al.* developed a hemostatic dressing based on poly(sodium acrylate), which demonstrated the ability to aggregate erythrocytes and alter cell morphology, ultimately resulting in accelerated blood clotting at the wound site.[19] On the other hand, Hall *et al.* developed a superabsorbent powder based on poly(sodium acrylate) with antibacterial properties against *S. aureus*, *E. coli*, and *P. aeruginosa* for treating localized infections.[20] The authors demonstrated that the produced medical powder showed no cytotoxicity towards fibroblasts. Poly(sodium acrylate) has also been employed in the fabrication of biocompatible materials using SLA (stereolithography) printing for biomedical applications, including its use in stents. In our study, we combined the unique superabsorbent properties of poly(sodium acrylate) with calcium-ion-saturated curdlan to create a layered dressing insert, which, firstly, absorbs excess exudate (and thus inflammatory mediators) and, secondly, accelerates the regeneration process (by stimulating the viability and proliferation of fibroblasts due to the presence of calcium ions). When tissues are damaged, calcium is released from damaged cells, serving as an activation signal for skin cells. In addition, calcium affects the ability of cells to adhere to other cells and structures and also plays a role in regulating cell proliferation, *i.e.*, their division, and contributes to the formation of new tissue and, as a result, accelerates the regeneration process.[21–23]

## 2 Materials and methods

### 2.1. Preparation of biomaterials

The biomaterials were synthesized following the procedure described in Polish Patent No. 246959 ("Method of producing a dressing insert based on curdlan for medical applications"). A schematic overview of the fabrication steps is presented in Fig. 2a–h. Four formulations were prepared and designated as Construct P1, Construct P2, Construct Cur_P1, and Construct Cur_P2. Constructs P1 and P2 were prepared without dialyzed curdlan enriched with calcium ions, whereas Constructs Cur_P1 and Cur_P2 contained this component. Benzophenone was used as the photoinitiator in P1 and Cur_P1, while benzoin served as the photoinitiator in P2 and Cur_P2.

**2.1.1. Preparation of poly(sodium acrylate-*co*-acrylic acid) – Constructs P1 and P2.** Acrylic acid (AAc) was neutralized with sodium hydroxide (NaOH) at an 85% molar ratio while maintaining the temperature below 10 °C to obtain a sodium acrylate (NaAc) solution (Fig. 2a). Glycidyl methacrylate (GMA) was then introduced as a crosslinking agent at a molar ratio of 1 : 100 relative to the initial amount of AAc. Subsequently, the appropriate photoinitiator benzophenone for Construct P1 or benzoin for Construct P2 was added at 0.5 wt% of the initial AAc mass (Fig. 2b).

The photopolymerization process was conducted under UV irradiation for 60 min (Fig. 2c). The resulting polymeric hydrogel was dried at 100 °C for 24 h and then milled in a vibratory ball mill to obtain a fine polymer powder (poly(NaAc-*co*-AAc)) (Fig. 2d and e).

The polymer powder was suspended in a 5 wt% ethanolic solution of polyvinylpyrrolidone (PVP) to form a printable bioink.

For the printing process extruder toolhead for paste-like materials was used. It enables 2D and 3D printing of dense masses which are extruded at high pressure through an exchangeable nozzle. After designing the constructs, we imported a DXF file to the Voxelizer Software (ZMorph S. A, Poland) and set parameters as follows (layer count: 2, layer height: 1 mm, print speed 10 mm $s^{-1}$). After generating the G-code we manually loaded the syringe extruder with the material, mounted it at the printer carriage mount and conneted by cables to the machine and proceeded with the printing. Path design was based on two perpendicular layers, each 1 mm thick, deposited in a grid pattern on the flat substrate to maximise


Fig. 1 Optical images of as printed structures (A and B), (C) cross-section image magn. 500×, (D) 3D surface reconstruction of the cross-section surface. Surface topography images of as printed construct were recorded using the digital optical microscope (VHX-7000, Keyence, Japan) with a DIC (VH-Z100UT) varifocal lens for roughness profile measurement and creating 3D model of the surface at magnification of 500×.

porosity and mechanical integrity of the structure. As a result, brittle structures of 8 mm × 5 mm were obtained. Due to the rheological properties of the paste and high water absorption capacity fibers were partially merged. The printing resolution, as defined by the layer height was 1 mm. However, the actual detail and sharpness of the structure was influenced by the material properties, leading to some merging of fibers and potentially reducing the effective resolution (Fig. 1).

**2.1.2. Preparation of curdlan-containing constructs – Constructs Cur_P1 and Cur_P2.** Curdlan hydrogel (Cur_11%) containing calcium ions was prepared according to the previously described method. The hydrogel was subsequently milled in a vibratory ball mill to obtain a powder form (Fig. 2f).

In parallel, crosslinked poly(sodium acrylate-*co*-acrylic acid) was synthesized using the same procedure as for Constructs P1 and P2. Benzophenone (for Cur_P1) or benzoin (for Cur_P2) was

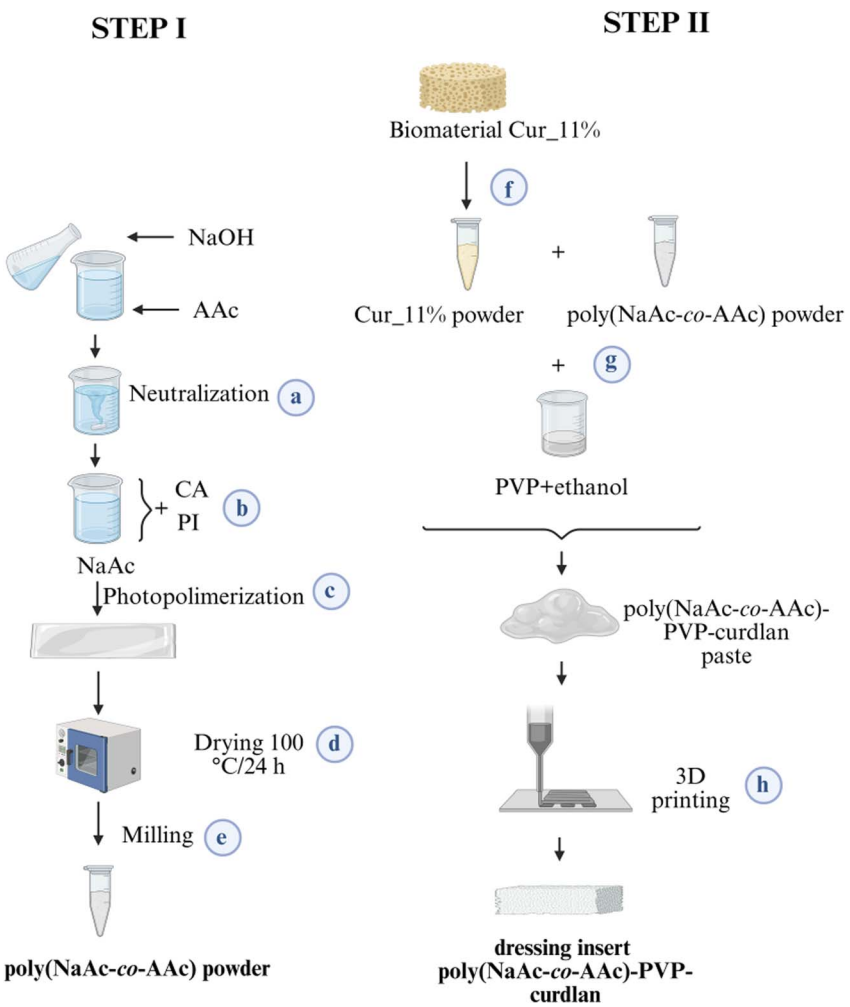


Fig. 2 The schematic process of manufacturing dressing inserts (Construct Cur_P1 and Construct Cur_P2). The illustration was created using biorender.com.

added as a photoinitiator at 0.5 wt% of the initial AAc mass. (Fig. 2a–e). The powders of Cur_11% and SAP were combined in a 5 wt% ethanolic PVP solution to yield a homogeneous bio-ink (Fig. 2g).

The resulting pastes were 3D printed into two perpendicular layers (1 mm each) using the same printing parameters as above, forming composite wound dressing inserts based on poly(NaAc-*co*-AAc)-PVP-curdlan (Fig. 2h). All other printing parameters and nozzle size were the same as for P1 and P2 constructs preparation procedure.

For enhanced visualization, the production procedure of the wound dressing insert was depicted graphically in Fig. 2.

### 2.2. Detailed characterization of biomaterials

**2.2.1. ATR-FTIR spectroscopy.** ATR-FTIR spectra of the samples were collected using the attenuated total reflection technique and a Bruker Tensor 27 FT-IR spectrophotometer (Bruker, Mannheim, Germany). For each sample, 32 scans were performed at 4 $cm^{-1}$ resolution in absorbance mode. Spectra were obtained in the wavenumber range from 400 to 4000 $cm^{-1}$.

**2.2.2. Differential scanning calorimetry (DSC) analysis.** Differential scanning calorimetry was analyzed using a Netzsch 204 DSC calorimeter (Netzsch, Günzbung, Germany). Samples of 8–10 mg were placed in an aluminum crucible. An empty aluminum crucible was used as a reference sample. Dynamic scanning was performed in a double pass with a temperature increment of 10°C $min^{-1}$. The first step was carried out in the range 25 °C–150 °C to remove absorbed water, while the second. Stage was carried out in the temperature range from 25 to 500 °C.

**2.2.3. TGA/DTG.** A TGA analysis was conducted using a Netzsch STA 449 F1 Jupiter thermal analyzer (Netzsch, Selb, Germany). The following analysis parameters were used: temperature rise 10 °C $min^{-1}$, gas flow 20 $cm^3$ $min^{-1}$ (helium atmosphere), temperature range 25 °C–600 °C, sample mass 10–12 mg. Measurements were carried out in an aluminum crucible, using an empty crucible as a reference sample.

**2.2.4. Surface topography.** The surface topography of samples was analyzed using scanning electron microscopy SEM (Ultra Plus GEMINI, Carl Zeiss, Jena, Germany). Before imaging, the samples were sputtered with a layer of carbon with an average thickness of 10 nm to ensure the flow of charge from the sample surface to the stage. The measurements were taken at an accelerating voltage of 2 kV and magnifications of 3000× and 5000×, respectively.

**2.2.5. Atomic force microscopy and optical surface profilers.** The images were taken using the Veeco (Plainview, NY, USA) NanoScope V AFM Atomic Force Microscope. The microscope enables the observation of the surface of solids in magnification and three dimensions and the visualization of the nanomechanical properties of the materials under investigation. The experiments were repeated 3 times for each sample. The average roughness ($R_a$) parameter was determined.

**2.2.6. Contact angle.** The study of static water contact angle (WCA) was conducted using deionized water with a conductivity of 0.09 μS $cm^{-1}$ and a goniometer (model DSA25B, Krüss, Hamburg, Germany). This method involves observing a liquid droplet placed on a flat sample, such as a textile or wound dressing, and directly measuring the contact angle with the surface.[24] The droplet shape was recorded directly by a digital camera and processed using the Krüss ADVANCE computer program (Krüss, Hamburg, Germany). The Young–Laplace equation was employed in the analysis of the droplet shape. Measurements were carried out by applying ten 10 μl of the droplets onto the sample set perpendicular to the dosing needle.

**2.2.7. Calcium ion-releasing ability.** The ability of biomaterials to release calcium ions was assessed in extracts prepared according to the guidelines of ISO 10993-5:2009.[25] For this purpose, biomaterials weighing 100 mg were placed in a 12-well plate, and 1 mL of EMEM medium with the addition of 2% FBS was added to each well. The biomaterials were incubated for 24 hours at 37 °C, 5% $CO_2$, and 95% humidity (Heraeus Cytoperm 2, Thermo Scientific, Waltham, MA, USA). EMEM medium incubated without biomaterials served as the control experiment. The concentration of calcium ions in the collected extracts was assessed using a calcium ion detection kit (Calcium CPC BioMaxima, Lublin, Poland) following the manufacturer's recommendations.

**2.2.8. Water vapor transmission test.** The ability of biomaterials to transmit water vapor was evaluated according to the gravimetric method, as described in detail previously.[23] The WVTR [g per $m^2$ per day] was calculated using the following equation:

$$\mathrm{WVTR} = \frac{W_w - W_d}{S}$$

where $W_w$ is the weight of the vial with wet silica gel (after 24-h incubation), $W_d$ is the weight of the vial with dry silica gel (before incubation), and $S$ is the surface area of the mouth of the vial ($m^2$).

**2.2.9. Wound exudate absorption capacity.** The ability of biomaterials to absorb simulated wound fluid (SWF) was evaluated according to the procedure described in detail previously.[23] The biomaterials designated for the study contained an equal amount of supersorbent component. The absorbent capacity of the biomaterials was determined based on the increase in their weight over time, according to the equation:

$$\mathrm{SW}(\%) = \frac{(W_s - W_d)}{W_d} \times 100$$

where, $W_s$ represents the mass of the swollen biomaterials (in grams), and $W_d$ represents the mass of the dried ones (in grams).

**2.2.10. Biocompatibility *in vitro*: viability, proliferation, and type I collagen production.** The cell culture experiments were conducted using normal human skin fibroblasts (BJ cell line – ATCC CRL-2522, London, United Kingdom), which serve as a model for assessing wound healing processes *in vitro*. The cells were cultured in the ATCC–recommended medium, Eagle's Minimum Essential Medium (EMEM from ATCC, Manassas, VA, USA), supplemented with 10% FBS (Pan-Biotech, Germany), and 100 U $mL^{-1}$ penicillin, and 100 μg $mL^{-1}$

streptomycin (Sigma-Aldrich, USA). The cultures were incubated at 37 °C in a humidified atmosphere with 5% $CO_2$ and 95% air (Heraeus Cytoperm 2, Thermo Scientific, Waltham, MA, USA). Extracts from the tested biomaterials were prepared according to ISO 10993-5:2009 (ref. 25) standards, with the concentration of FBS added to the culture medium varying depending on the analysis being performed: EMEM supplemented with 2% FBS was used to assess cell viability, while EMEM supplemented with 10% FBS was used to assess cell proliferation.

*2.2.10.1 Assessment of cell viability.* The cell viability assay was conducted according to the procedure described earlier.[15] In brief, fibroblasts were seeded onto 96-well plates at a concentration of $1.5 \times 10^5$ cells per mL in EMEM medium supplemented with 10% FBS. After 24 hours of incubation, the culture medium above the cells was gently removed and replaced with extracts from the biomaterials. The plates were then incubated for another 24 and 48 hours. Cell viability was assessed using the MTT assay, and additionally, fibroblasts were stained with fluorescent dyes (using the live/dead assay kit according to the manufacturer's instructions). The results of the MTT assay were presented as the percentage of absorbance values relative to those obtained with the negative control (polystyrene extract – EMEM without sample). Additionally, stained cells were observed using a confocal laser scanning microscope (CLSM, Olympus FluoView equipped with FV1000, Shinjuku, Japan).

*2.2.10.2 Assessment of cell proliferation.* Cell proliferation assessment was conducted using the indirect method, utilizing extracts from the fabricated biomaterials prepared in EMEM supplemented with 10% FBS. BJ cell line cells were seeded onto 96-well plates at a density of $2 \times 10^4$ cells per mL in a volume of 100 μL. After 24 hours of incubation, the culture medium above the cells was gently removed and replaced with extracts from the biomaterials. The plates were then incubated for 3 and 5 days, respectively. Following the specified incubation periods, cell proliferation was assessed using the WST-8 assay (Sigma-Aldrich, USA). The fold increase in cell proliferation was calculated according to the equation:

$$\text{Fold increase in cell proliferation} = \frac{b-a}{a}$$

where "*a*" represents the value of optical density (OD) acquired for the tested group on day three, while "*b*" represents the value of OD obtained for the tested group on day five.

On the fifth day (after completion of the quantitative test), the cells were fixed in a 3.7% formaldehyde solution, subsequently treated with a 0.2% Triton X-100 solution, and blocked with 1% BSA (all reagents used were purchased from Sigma-Aldrich Chemicals, Warsaw, Poland). The cells were then stained with fluorescent dyes Hoechst 33 342 and Alexa Fluor™ 635 Phalloidin (Invitrogen Warsaw, Poland) and examined using confocal laser scanning microscopy (CLSM) equipped with an Olympus FluoView FV1000 system in Shinjuku, Japan.

*2.2.10.3 Type I collagen production.* To qualitatively assess the production of collagen by BJ cells, the cells were seeded as for the proliferation assay and cultured for five days, with half of the medium changed every three days. Subsequently, the cells were fixed and blocked with BSA (as described above). Human-specific antibodies against collagen type I were added to these prepared cells and incubated for 16 hours at 4 °C. After this time, the primary antibodies were removed from the wells, the cells were washed with PBS, and then incubated with Alexa Fluor™ 647 – conjugated secondary antibodies (Invitrogen, Warsaw, Poland). Additionally, the cells were stained with DAPI for visualization of cell nuclei. Observations were conducted using CLSM.

**2.2.11. Assessment of mutagenicity *in vitro*.** Bacterial Reverse Mutation Test (Ames assay) The Ames assay was performed according to OECD Guideline 471: Bacterial Reverse Mutation Test. The Ames test was performed according to the original manufacturer's instruction – Muta-Chromo Plate, Bacterial Strain KIT (EBPI), and described in detail previously.[26,27]

The assay was performed on biomaterials extracts obtained as described in Section 2.2.10. Two strains of *Salmonella typhimurium* with different mutations in their DNA were used for the test: TA 100 (CIP 103799), containing a base pair substitution mutation, and TA 98 (CIP 103798), containing a frameshift mutation. His- *Salmonella typhimurium* strains were incubated with the tested extracts, both in the presence and absence of exogenous metabolic activation (S9 fraction), using a medium without histidine. After incubation, the number of revertant wells per plate was counted. Next, the ratio between the surviving control bacteria not exposed to the mutagen and the surviving experimental bacteria that were exposed to the mutagen was calculated.

**2.2.12. Blood compatibility tests: hemolysis and blood clot formation test.** Blood was collected from a healthy volunteer with the approval of the Bioethics Committee of the Medical University of Lublin (approval no. KE-0254/258/2020) using citrate. The procedures were carried out according to the protocol described by Michalicha *et al.*[28] The concentrations of total hemoglobin and plasma hemoglobin were estimated based on the reaction with Drabkin's reagent and an appropriate calibration curve, using 96-well plates and a Synergy H4 hybrid microplate reader (Agilent Technologies, Santa Clara, CA, USA). The results were 138 mg% and 0.19 mg $mL^{-1}$, respectively. For the hemolysis test, biomaterial samples weighing 30 mg ± 2 mg were immersed in 2 mL of blood diluted 100× in PBS at pH 7.4, without $Ca^{2+}$ and $Mg^{2+}$ ions. The positive control contained 0.1% Triton X-100, while the negative control consisted of 30 mg ± 2 mg HDPE (Sigma-Aldrich, USA). The biomaterials were incubated for 3 hours at 37 °C in an Innova 42 shaking incubator (New Brunswick Scientific, Edison, NJ, USA) at 150 rpm. The hemoglobin released by erythrocytes was estimated using a reaction with Drabkin's reagent, as described above. To verify the clot-forming ability of the biomaterials, 100 μL of whole blood activated with 10 mM $CaCl_2$ was dripped onto the surfaces of the biomaterials (each weighing 30 mg ± 2 mg). HDPE served as the negative control, while non-activated, $Ca^{2+}$-free whole blood (100 μL) was used as the positive control. The biomaterials were incubated for 30 minutes at 30 °C. Subsequently, the samples were incubated with 2.5 mL of distilled

 

water for 5 minutes. The hemoglobin content in the solution was determined using Drabkin's reagent reaction. Each experiment was conducted in triplicate. Statistically significant differences between the negative control and the samples were analyzed at a significance level of $p < 0.0001$.

**2.2.13. Statistical analysis.** Statistically significant differences between various samples were considered calculated according to a One-way ANOVA with post-hoc Dunnett's test, Tukey test or Tukey test, using GraphPad Prism 8.0.0 Software (GraphPad, La Jolla, CA, USA). Samples were used in different numbers for various tests, but at least in triplicate (details in appropriate sections). Each experiment was conducted independently three times, and data are expressed as mean ± standard deviation ($n = 3$).

# 3 Results and discussion

## 3.1. ATR-FTIR

Fig. 3 shows the FTIR/ATR spectrum of the materials tested. For all analyzed compositions, stretching vibrations originating from the hydroxyl group (in the range 3389–3408 $cm^{-1}$) are visible. Stretching vibrations of C–H in the 2927–2947 $cm^{-1}$ range could be observed. Two strong signals corresponding to the pyrrolidone unit are visible: stretching vibrations from the tertiary amide group (1534–1576 $cm^{-1}$), probably connected with homopolymer of PVP and N–C=O stretching vibration (1653–1657 $cm^{-1}$) from the PVP lactam ring. At 1033–1037 $cm^{-1}$ C–O groups stretching vibrations are also noticed. C–H asymmetric deformation vibration at 1411–1424 $cm^{-1}$ could also be observed.

A comparison of the wavenumbers of the characteristic bands is given in Table 1.

**3.1.1. The obtained FTIR-ATR analysis results indicate the following statements.** The FTIR-ATR spectra confirmed the presence of characteristic functional groups in the investigated materials. A broad absorption band observed at 3389–3408 $cm^{-1}$ corresponds to the stretching vibrations of hydroxyl groups, which are typical of curdlan. These groups are known to form hydrogen bonds that enhance the material's water and moisture absorption capacity.[29,30] The bands observed at 2927–2947 $cm^{-1}$ are attributed to the stretching vibrations of C–H bonds, which may originate from both curdlan and PVP, as these polymers contain aliphatic chains.[31] Signals at 1534–1576 $cm^{-1}$ and 1653–1657 $cm^{-1}$ are assigned to the stretching vibrations of tertiary amide groups and lactam rings, respectively. These features are characteristic of PVP, which contributes to the hydrogen bonding capacity of the material through its amide moieties, thereby enhancing its moisture retention properties.[32] The bands detected at 1033–1037 $cm^{-1}$ correspond to C–O stretching vibrations and are likely derived from both

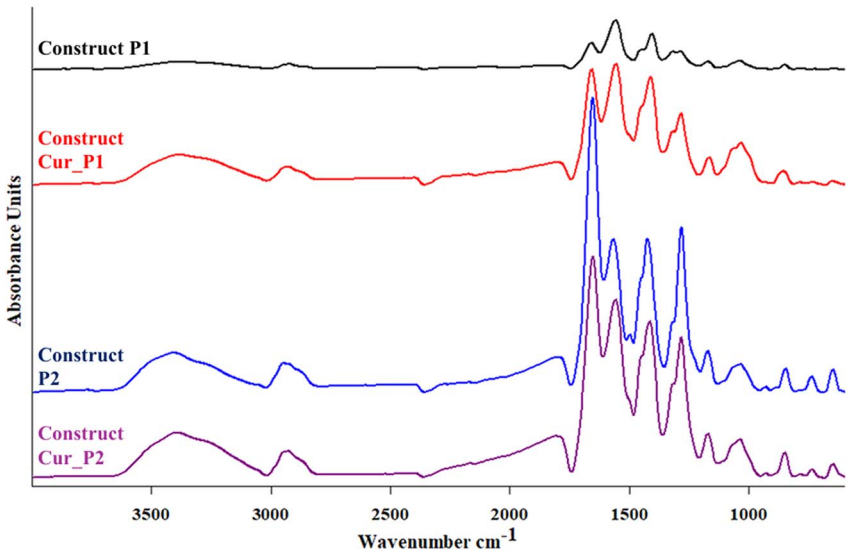


Fig. 3 FTIR/ATR spectrum of synthesized materials.

Table 1 Wavenumber of the selected band visible in FTIR spectrum corresponding to the specific elements of the chemical structure

| | Wavenumber [$cm^{-1}$] | | | | | |
|---|---|---|---|---|---|---|
| Sample | Hydroxyl group | Hydrocarbon group | Tertiary amide group | Lactam ring | Carbonyl group | Hydrocarbon group |
| Construct Cur_P1 | 3397 | 2929 | 1534 | 1653 | 0937 | 1414 |
| Construct Cur_P2 | 3389 | 2927 | 1557 | 1657 | 1033 | 1411 |
| Construct P2 | 3407 | 2949 | 1568 | 1654 | 1035 | 1425 |
| Construct P1 | 3408 | 2947 | 1576 | 1653 | 1034 | 1424 |

curdlan and poly(sodium acrylate-*co*-acrylic acid). These groups are common in hydrophilic polymers and contribute to water absorption.[30,33] Additionally, the presence of asymmetric deformation vibrations of C–H bonds at 1411–1424 $cm^{-1}$ indicates contributions from all three polymeric components. These vibrations are associated with the structural flexibility and stability of the polymer matrix, which are essential features of effective wound dressing materials.[33]

### 3.2. Differential scanning calorimetry

For Construct P2 and Construct P1, two endothermic effects were visible, the first at about 278 °C and the second at 436 °C, and correlated with sample degradation. For Construct_Cur P2 and Construct Cur_P1, two effects were apparent. The first was exothermic, visible at approximately 245 °C, and likely due to the crosslinking reaction of the samples. The second effect exhibited an endothermic character, visible at approximately 436 °C, and originated from the total degradation of the sample (Fig. 4).

These results can be directly linked to the FTIR analysis, which indicates the presence of hydroxyl and amide groups responsible for the material's ability to absorb moisture. Crosslinking, confirmed by the exothermic effect in DSC, increases the stability and strength of the material, which is crucial for its mechanical properties and durability. The high degradation temperature (436 °C) suggests that the material is thermally stable and can withstand sterilization processes, such as steam sterilization in an autoclave, which occurs at temperatures of 121 °C–134 °C.

The ability to withstand such temperatures without significant degradation means that this biomaterial is suitable for medical applications where high-temperature sterilization is required while maintaining its absorptive and mechanical properties. Thus, this biomaterial combines both a high degree of sterility and efficiency in moisture management as well as structural stability, making it an ideal candidate for advanced applications in medical dressings.[34]

### 3.3. TGA/DTG

The decomposition of Construct P1 occurred in three stages. The first decomposition was observed at 194.0 °C and corresponded to a mass loss of 18.49%, the second at 426.7 °C (13.42% weight loss), while at 453.2 °C (21.97% weight loss). It was the most thermally stable system, with temperatures of $T_{5\%}$ and $T_{50\%}$ being the highest among the other materials tested. They were 152.1 °C and 481.8 °C, respectively. The first decomposition peak relates to the degradation of the ester part. The second and third degradation peaks correspond to the total degradation of aliphatic C–C chains and PVP molecules. Construct P2 showed a similar decomposition pattern. The first decomposition temperature was 191.8 °C (weight loss was 11.34%), the second decomposition was 425.2 °C (14.29% weight loss), and the third decomposition was 452.6 °C (22.28% weight loss). Construct_Cur P1 decomposed into 4 stages. The first decomposition temperature was 163.6 °C (12.74% mass loss), the second 255.2 °C (16.2% mass loss), the third 414.6 °C (11.04% mass loss), and the fourth 437 °C (18.28% mass loss). The least thermally stable was Construct Cur P2. This system also decomposed in four stages, with a first decomposition temperature of 108.1 °C (8.97% mass loss). The second decomposition temperature was 252.6 °C (24.93% mass loss), the third 416.1 °C (11.66% mass loss), and the fourth 435.9 °C (13.82% mass loss). This system also had the lowest $T_{5\%}$ and $T_{50\%}$ values. This indicates that the addition of curdlan reduced the thermal stability of the systems (Table 2).

Constructs P1 and P2 (Fig. 5) exhibit higher thermal stability than other biomaterials (Cur_P1 and Cur_P2), suggesting that they may be more resistant to sterilization processes. The high $T_{5\%}$ and $T_{50\%}$ values indicate that these materials can withstand such conditions without significant degradation, which is crucial for maintaining their mechanical integrity and functionality as wound dressing material.

The addition of curdlan in the Cur_P1 and Cur_P2 constructs resulted in a decrease in thermal stability. However, despite the overall reduction in thermal stability due to the

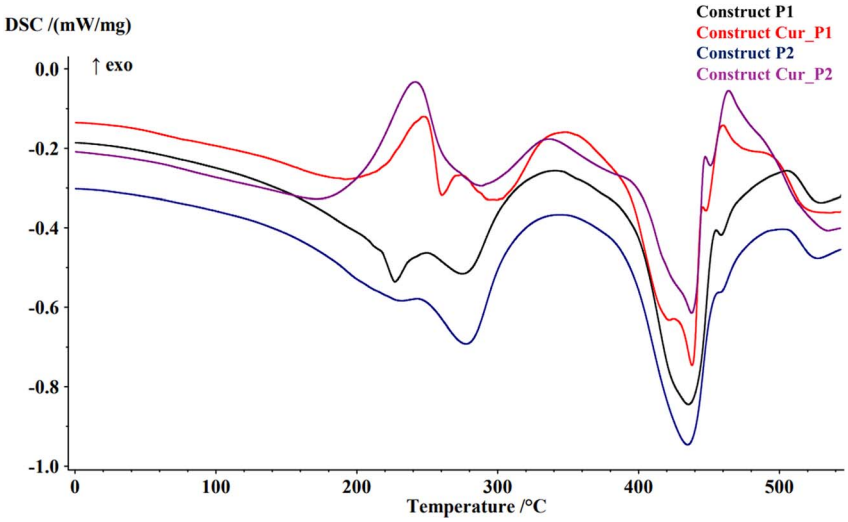


Fig. 4 DSC curves obtained for the samples.

Table 2 TGA/DTG data

| TGA/DTG | Construct P1 | Construct Cur_P1 | Construct P2 | Construct Cur_P2 |
|---|---|---|---|---|
| $T_{max_1}$ (°C) | 194.0 | 163.6 | 191.8 | 108.1 |
| $T_{max_1}$ mass loss (%) | 18.49 | 12.74 | 11.34 | 8.97 |
| $T_{max_2}$ (°C) | — | 255.2 | — | 252.6 |
| $T_{max_2}$ mass loss (%) | — | 16.3 | — | 24.93 |
| $T_{max_3}$ (°C) | 426.7 | 414.6 | 425.2 | 416.1 |
| $T_{max_3}$ mass loss (%) | 13.42 | 11.04 | 14.29 | 11.66 |
| $T_{max_4}$ (°C) | 453.2 | 437.0 | 452.6 | 435.9 |
| $T_{max_4}$ mass loss (%) | 21.97 | 18.28 | 22.28 | 13.82 |
| $T_{5\%}$ (°C) | 152.1 | 128.5 | 138.1 | 99.8 |
| $T_{50\%}$ (°C) | 481.8 | 455.8 | 473.1 | 443.0 |
| RM (%) | 46.12 | 41.64 | 52.09 | 40.62 |

addition of curdlan, Construct Cur_P2 remains adequately stable for use as a wound dressing material that can be sterilized with high-pressure steam. Thanks to the synergy between the FTIR and DSC results, this material combines high absorbent capacity with sufficient thermal stability, making it a valuable candidate for advanced medical applications where sterility and effective moisture management are required.

### 3.4. Surface topography

Surface topography analysis by scanning electron microscopy (SEM) revealed uniform and highly porous structures with micrometric pores (Fig. 6). A unique three-dimensional framework structure was visualized for all samples. In particular, the highly demanded feature of open porosity for absorbent materials was shown.

Wound dressings must exhibit the ability to rapidly absorb moisture, which is crucial for managing wound exudate and maintaining an appropriate healing environment.[35] Open porosities, as observed in the SEM images (Fig. 6), are highly desirable as they enable better fluid absorption. The three-dimensional framework structure visible in the samples potentially increases the surface area in contact with exudate, thereby accelerating the absorption process.

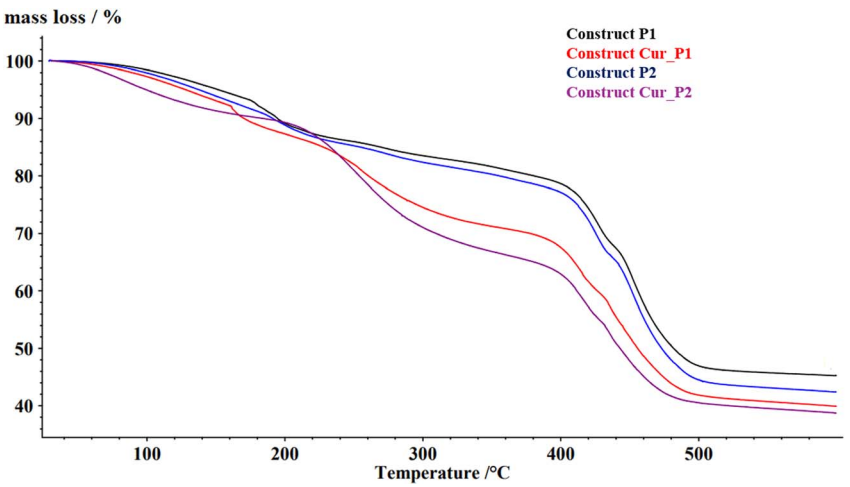


Fig. 5 TGA curves obtained for the samples.

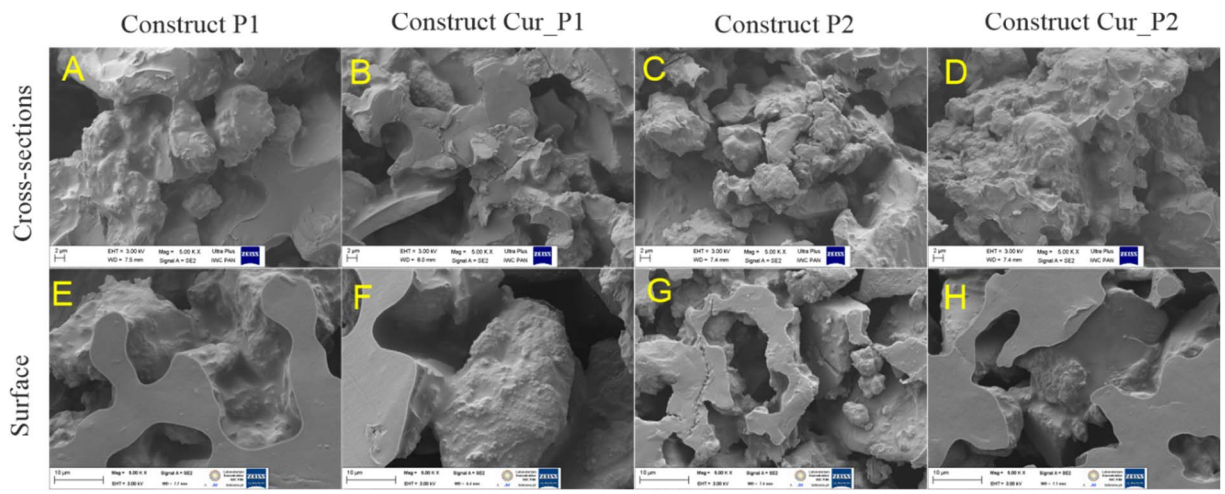


Fig. 6 SEM images of biomaterials with the magnification of 5000× for cross-sections (A–D) for surface view (E–H).

Moreover, such a porous structure also facilitates gas exchange, which is essential for delivering oxygen to the wound, thus supporting the healing process.[36] The differences between the samples indicate that the addition of curdlan leads to increased porosity and a three-dimensional structure, which is beneficial for wound dressing materials. In turn, the addition of

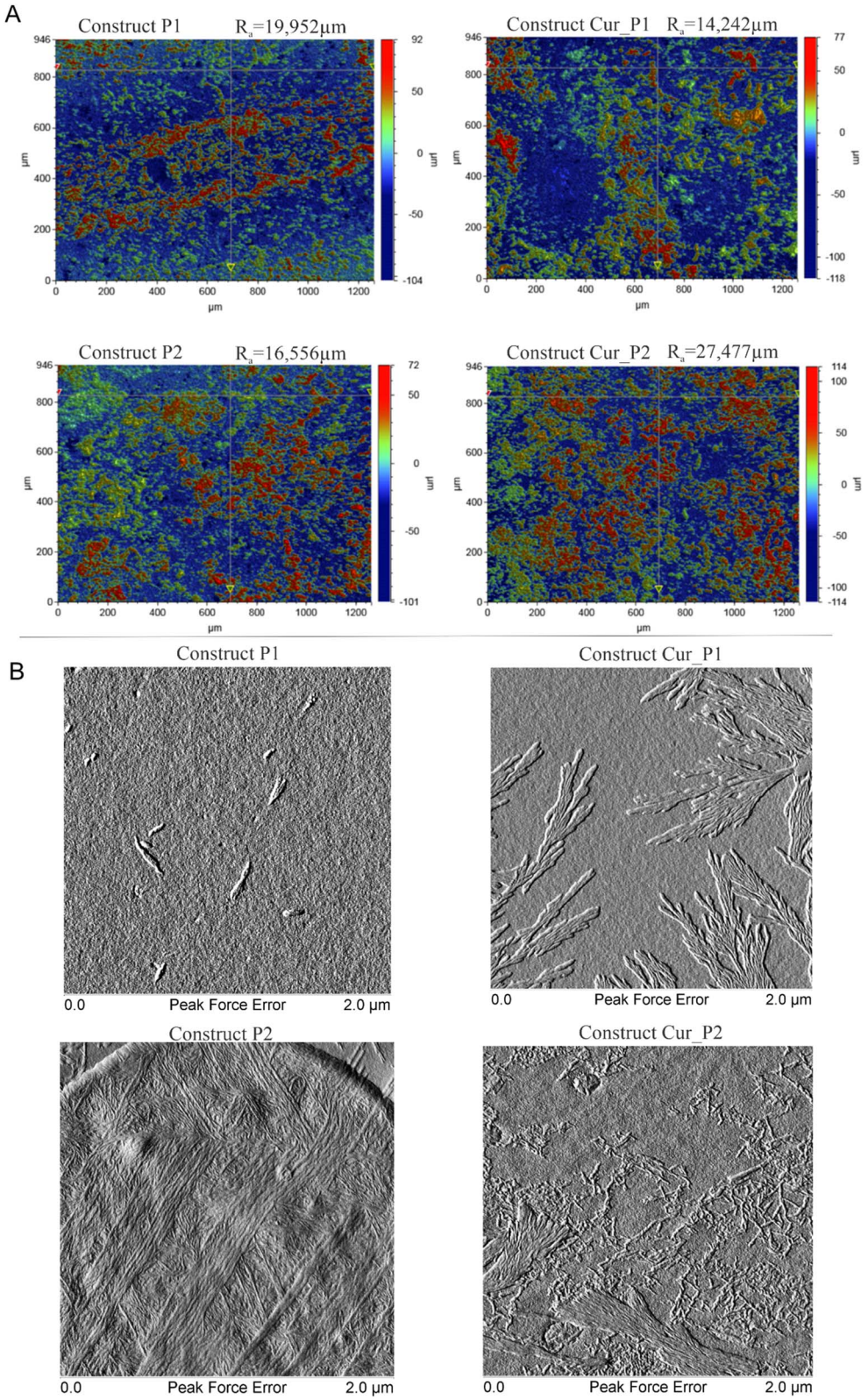


Fig. 7 (A) Profilometric 3D surface maps of Construct P1, Construct Cur_P1, Construct P2, and Construct Cur_P2 showing microscale roughness distribution. (B) AFM Peak Force Error images presenting nanoscale topographical features of the same constructs.

curdlan in the Cur_P1 and Cur_P2 constructs may reduce thermal stability, as previously mentioned, it simultaneously significantly enhances the absorbent properties and porosity, which are crucial for effective wound dressings.

### 3.5. Atomic force microscopy and optical surface profilers

In Fig. 7A, the profilometric analyses of the studied materials are presented, showing no significant changes in the surface of the materials are visible. The $R_a$ coefficient ranges from 14.242 μm (Construct Cur_P1) to 27.477 μm (Construct_Cur P2). The sample with curdlan exhibits the highest surface roughness among the others, and the system has the most heterogeneous surface. Additionally, a fragment of the parent composite surface examined using an atomic force microscope (AFM) is presented in Fig. 7B.

From the profilometric analysis (Fig. 7A), it can be concluded that there are no significant changes in the surface among the different samples in terms of overall roughness distribution. However, the samples with the addition of curdlan, particularly Construct Cur_P2, have higher $R_a$ values, which may influence their functional properties. AFM images (lower part of Fig. 7B) show differences in surface microstructure among the samples. Samples with curdlan (Cur_P1 and Cur_P2) exhibit more pronounced surface structures compared to the samples without curdlan. These structures may contribute to increased absorbent capacity of the wound dressing material by increasing the surface area in contact with fluids and better moisture retention. Surface roughness is a key factor influencing how well a wound dressing material adheres to the wound and how effectively it absorbs exudates. Too high a roughness could limit the contact surface, reducing absorption efficiency. On the other hand, too low roughness may lead to excessive adherence of the material to the wound, which could be problematic during dressing changes. The appropriate $R_a$ value for wound dressing materials depends on specific clinical requirements, but it generally should allow for effective fluid absorption without the risk of tissue damage during dressing changes. The $R_a$ values observed in the Cur_P1 and Cur_P2 samples, particularly the higher ones (*e.g.*, 27.477 μm for Cur_P2), may suggest good absorption while maintaining an appropriate balance between adhesion and ease of removal of the dressing. The heterogeneity of the surface in the curdlan-containing samples suggests that these materials may better handle different types of exudates and allow for better fluid drainage, which is important for dressings used on wounds that exude large amounts of fluid.

### 3.6. Contact angle

The obtained water contact angles for the samples were measured, and the results indicated visible changes in surface wettability (Fig. 8). Notably, samples containing the curdlan component (Construct Cur_P1, Construct Cur_P2) exhibited lower water contact angles compared to samples without curdlan (Construct P1, Construct P2). The addition of curdlan in both series of samples resulted in a lowering of the water contact angles.

The contact angle is a crucial parameter in evaluating wound dressing materials, as it determines the extent to which a material is hydrophobic or hydrophilic. A lower contact angle indicates that the material is more hydrophilic, which enhances the absorption of fluids such as wound exudate. In the context of wound dressings, materials with a low contact angle are

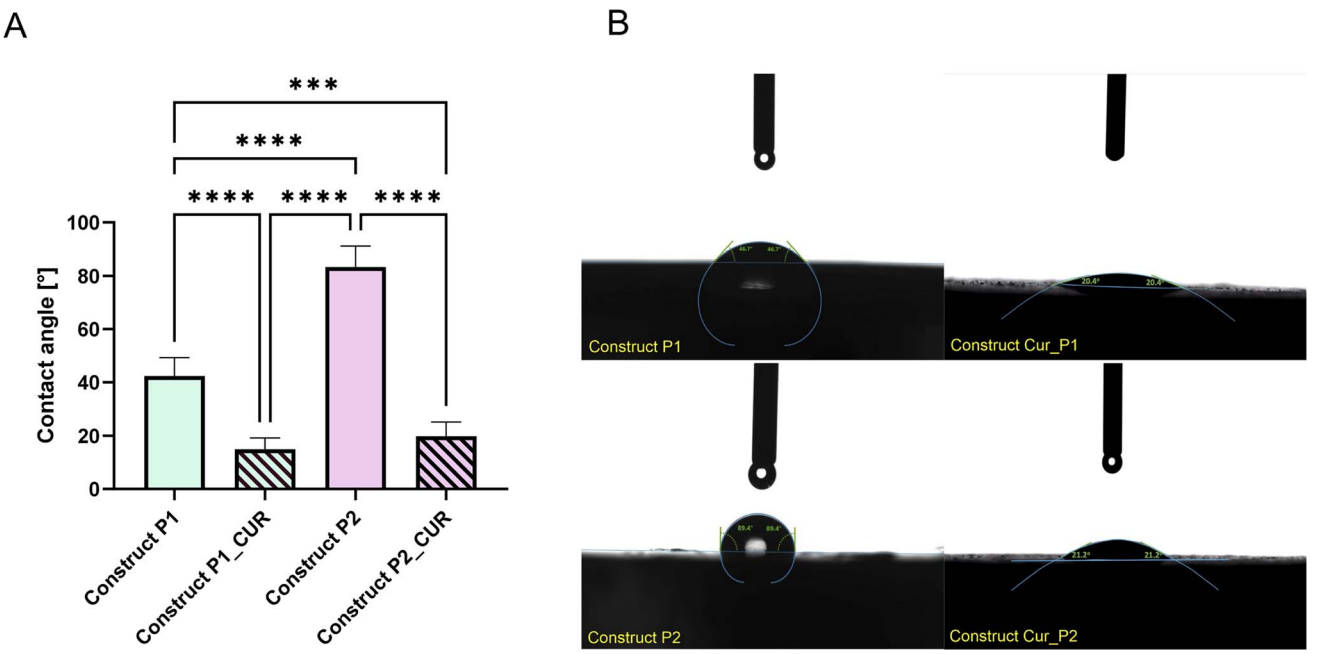


Fig. 8 (A) Water contact angle values measured for Construct P1, Construct Cur_P1, Construct P2, and Construct Cur_P2. Statistical analysis was performed using one-way ANOVA followed by Tukey's post-hoc test. The significance levels indicated on the graph correspond to pairwise comparisons identified as statistically significant by Tukey's test (***$p$ < 0.001, ****$p$ < 0.0001). (B) Representative side-view images of water droplets deposited on the surface of each construct, illustrating the corresponding contact angle measurements.

preferred because they absorb moisture more effectively, helping to maintain an optimal healing environment and preventing skin maceration around the wound.[37] Samples without the addition of curdlan (Construct P1 and Construct P2-Fig. 8) exhibit higher contact angle values (approximately 50° for P1 and up to 90° for P2), indicating that they are more hydrophobic. This suggests that these materials may be less effective at absorbing wound exudate, which could limit their efficiency as wound dressings. Samples containing curdlan (Construct Cur_P1 and Construct Cur_P2) display significantly lower contact angle values (below 30°), indicating a clearly hydrophilic character. Such materials are likely to be more effective in absorbing exudates, which is beneficial for creating the appropriate conditions for wound healing. The conclusions drawn from the contact angle analysis indicate that the addition of curdlan significantly improves the surface hydration of wound dressing materials, making them more effective in the context of fluid absorption. Materials with a lower contact angle are more desirable in medical applications because they promote the maintenance of appropriate moisture levels at the wound site, thereby supporting the healing process and minimizing the risk of infection.

### 3.7. The calcium ion-releasing ability

Calcium plays a key role in the wound healing process, acting as a regulator supporting the subsequent stages of coagulation. Starting from enzymatic reactions leading to the activation of prothrombin, through the formation of fibrin and platelet aggregation, to the formation of a stable blood clot. Considering the significant biological role of calcium ions, we used a curdlan-based hydrogel biomaterial enriched with the aforementioned ions in our studies. In our previous works, we showed that ion exchange dialysis allows the incorporation of various divalent metal ions into the biomaterial, depending on the salt used, and then their release into the external environment.[15,38,39]

To verify whether the method used for creating a bioink from the Cur_11% biomaterial does not interfere with the $Ca^{2+}$ release process, a calcium ion release test was performed for each of the printed biomaterials (Fig. 9). The result obtained after conducting the colorimetric analysis confirmed our assumptions. Only biomaterials produced using calcium-enriched curdlan, labeled as Constructs Cur_P1 and Cur_P2, exhibited the ability to release $Ca^{2+}$ ions. This indicates that the Cur_11% biomaterial can be successfully used as a bio-ink for 3D biomaterial production with medical potential. Due to its ability to release calcium ions, it has the potential to support the regenerative processes of damaged tissues. On the medical market, several commercial dressings are known to release calcium ions, such as Kaltostat® (ConvaTec), Algisite™ M (Smith & Nephew), and Sorbalgon® (Hartmann).[40–42] These materials promote coagulation primarily through $Ca^{2+}$ release and have been reported to stimulate fibroblast proliferation and migration *in vitro*, confirming the beneficial biological activity of calcium ions. In our previous work, we verified this effect experimentally by demonstrating that Kaltostat supported fibroblast viability and metabolic activity under *in vitro*

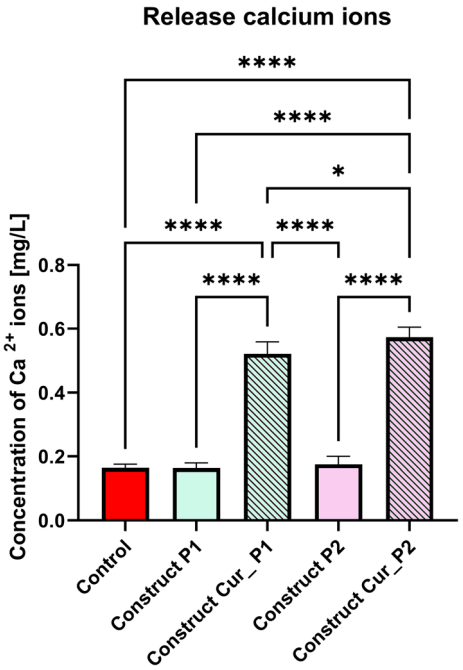


Fig. 9 Concentration of calcium ions released from Construct P1, Construct Cur_P1, Construct P2, and Construct Cur_P2 biomaterials after 24 h incubation in culture medium (EMEM supplemented with 2% FBS). Extracts were prepared according to ISO 10993-5:2009 recommendations. Statistical analysis was performed using one-way ANOVA followed by Tukey's multiple comparison test. Asterisks indicate statistically significant differences between the compared samples (*$p < 0.05$, ****$p < 0.0001$).

conditions.[15] However, such dressings rely almost exclusively on ion release and show limited fluid absorption capacity compared with our constructs. In the same study, we compared the absorption performance of the commercial calcium–alginate dressing Kaltostat, which contains $Ca^{2+}$ ions. Its dry mass increased by approximately 1000% after fluid uptake. Interestingly, other authors have reported that the fibrous structure of Kaltostat may be disadvantageous in wound healing because individual fibres can migrate into the wound bed, potentially delaying tissue regeneration.[43]

This observation highlights a distinct advantage of our material. Firstly, it also releases calcium ions, thereby supporting the coagulation process and fibroblast activity. Secondly, it exhibits a markedly higher absorption capacity compared with Kaltostat. Thirdly, unlike fibrous alginate dressings, the designed insert will be surrounded by protective outer layers, which prevents any material fragments from remaining in the wound bed and ensures safe removal after use.

### 3.8. Water vapor transmission test

According to the currently accepted paradigm of wound treatment, the fundamental requirement for dressings is the ability to control water loss, determined by the Water Vapor Transmission Rate (WVTR) coefficient. On the one hand, too low WVTR may lead to exudate accumulation and consequently to maceration of the regenerating tissue, as well as promote

 

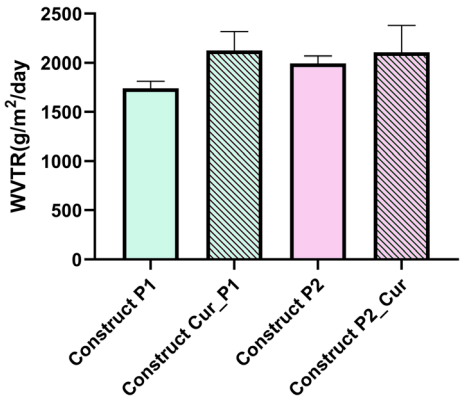


Fig. 10 The water vapor transmission rate coefficients for the printed biomaterials: Construct P1, Construct Cur_P1, Construct P2, Construct Cur_P2. No statistically significant differences were observed between the tested samples ($p > 0.05$).

colonization by pathogenic microorganisms. On the other hand, excessively high WVTR levels may result in dehydration of the wound bed and adherence of the biomaterial to the damaged tissue, and could cause painful dressing changes. Based on *in vitro* and *in vivo* studies, Xu *et al.* determined that a dressing with a WVTR of approximately 2028.3 g per $m^2$ per 24 h allows for maintaining an optimal moisture level for epidermal cell proliferation.[44]

The conducted study aimed at determining the water vapor transmission rate (WVTR) coefficient revealed that each of the tested biomaterials exhibited an optimal WVTR for wound healing, close to 2028.3 g per $m^2$ per 24 h (Fig. 10). The addition of calcium-enriched curdlan to the biomaterial constructions increased the WVTR coefficient (for construct Cur_P1, WVTR = 2123.12 g per $m^2$ per 24 h; for construct Cur_P2, WVTR = 2104.88 g per $m^2$ per 24 h). WVTR of approximately 2028.3 g per $m^2$ per 24 h, which has been reported to provide an optimal moist environment and to enhance fibroblast and keratinocyte proliferation in three-dimensional wound dressings.[45] The obtained results of the WVTR coefficient allow us to assume that printed biomaterial constructs with the addition of curdlan will have a positive effect on the cell proliferation process and therefore, will subsequently positively influence the regeneration of damaged tissues, which remains to be proven.

### 3.9. Wound exudate absorption capacity

A biomaterial intended for exuding wounds should absorb excess exudate while simultaneously maintaining moisture balance within the wound bed. Furthermore, the absorbed exudate (along with any entrapped microorganisms) should be

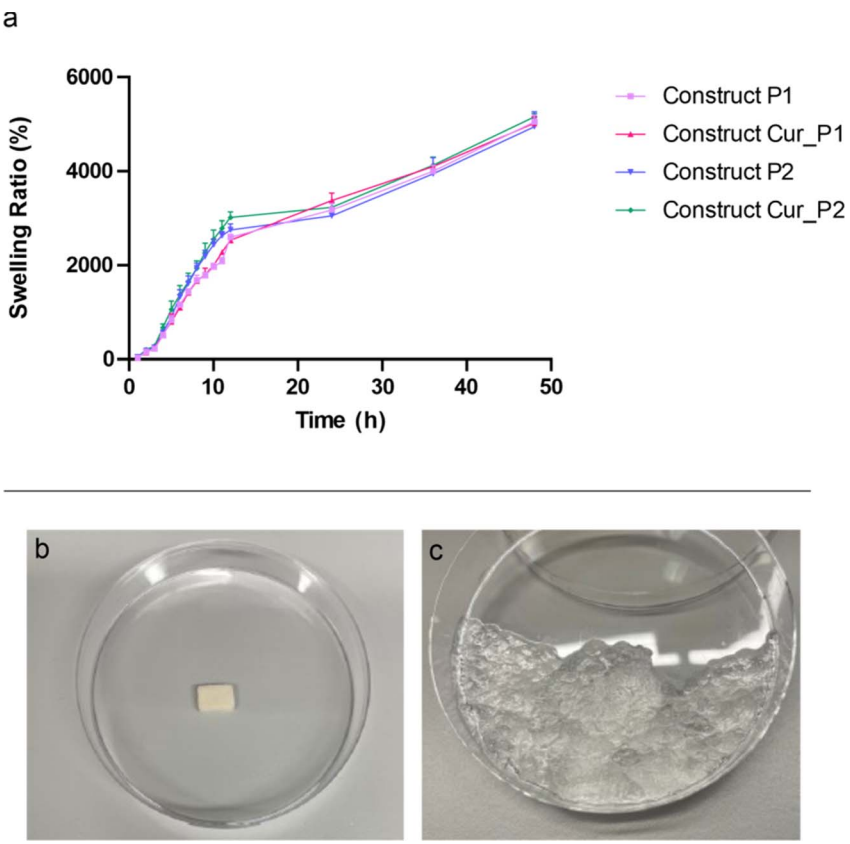


Fig. 11 (a) The capacity of Construct P1, Construct Cur_P1, Construct P2, and Construct Cur_P2 to absorb simulated wound fluid (SWF), expressed as a percentage increase in initial mass; (b) representative photograph of Construct Cur_P2 biomaterial in its dry state; (c) representative photograph of Construct Cur_P2 biomaterial in a state of full saturation with simulated wound fluid (after 48 h). No statistically significant differences were observed between the tested samples ($p > 0.05$).

retained within the biomaterial structure to prevent reinfection and maceration of the regenerating tissue. Superabsorbent polymers (SAPs), by absorbing aqueous solutions (including exudate), can swell and increase their volume until reaching complete saturation. They do not dissolve or release the absorbed fluid even under external pressure (*e.g.*, compression).[16] The conducted experiment aimed to demonstrate that each of the fabricated biomaterials exhibited significant absorbent properties (see Fig. 11A). It turned out that each of the fabricated constructs increased its mass by approximately 5000% compared to the biomaterials in their initial (dry) state (Calculated values of mentioned earlier SW factor are: Construct P1 = 5051.84 ± 68.24%, Construct Cur_P1 = 5022.41 ± 63.41%, Construct P2 = 4945.32 ± 62.98%, Construct Cur_P2 = 5159.46 ± 67.61%). The addition of curdlan did not significantly affect the absorbent properties of the produced constructs. Furthermore, the biomaterials underwent gradual saturation, with saturation plateauing after 48 hours (Fig. 11C). It should be noted that the developed material is designed as an absorbent insert for multilayer wound dressings, similar in concept to commercial products such as DryMax® Extra, Exufiber®, or Cutisorb® Super, which rely on superabsorbent polymer cores enclosed within protective outer layers. However, these existing materials are bioinert and serve only as passive exudate absorbers. In contrast, the curdlan-based insert described here combines high absorbency with potential bioactivity, owing to

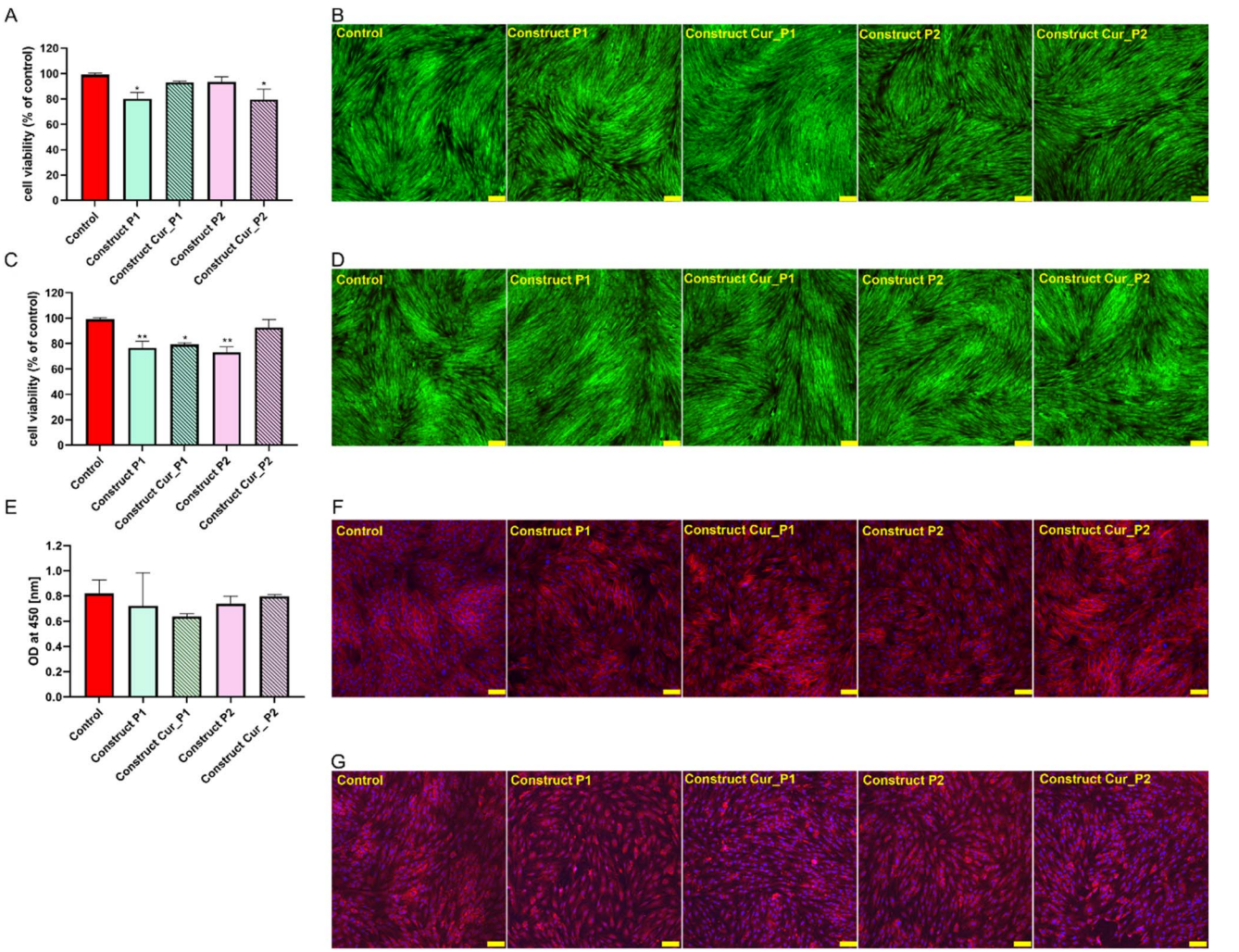


Fig. 12 (A) Cell metabolic activity assessed by the MTT assay after 24 h incubation with biomaterial extracts. Asterisks indicate statistically significant differences compared to the control extract (*$p < 0.05$, **$p < 0.01$), according to one-way ANOVA followed by Dunnett's post-hoc test. (B) Live/dead CLSM images of cells after 24 h incubation with biomaterial extracts, showing viable (green) and dead (red) cells. Magnification 100×; scale bar = 100 μm. (C) Cell metabolic activity assessed by the MTT assay after 48 h incubation with biomaterial extracts. Asterisks indicate statistically significant differences compared to the control extract (*$p < 0.05$, **$p < 0.01$), according to one-way ANOVA followed by Dunnett's post-hoc test. (D) Live/dead CLSM images of cells after 48 h incubation with biomaterial extracts. Magnification 100×; scale bar = 100 μm. (E) Cell proliferation evaluated using the WST-8 colorimetric assay after 5 days exposure to biomaterial extracts. No statistically significant differences were observed between the samples and the control ($p > 0.05$). (F) CLSM images of cells cultured for 5 days in the presence of the extracts, showing nuclei (blue, Hoechst 33 342) and cytoskeletal filaments (red, AlexaFluor™ 635-phalloidin). Magnification 100×; scale bar = 100 μm. (G) Immunofluorescent CLSM visualization of type I collagen deposition after 5 days of culture (red), with nuclei counterstained in blue. Magnification 100×; scale bar = 100 μm.

the presence of calcium-enriched curdlan, which may contribute to improved wound healing and tissue regeneration.[46]

### 3.10. Biocompatibility tests *in vitro*

The final stage of the conducted research involved assessing the impact of extracts from the produced dressing inserts (24- and 48-hour incubation) on normal skin cells (BJ cell line, ATCC CRL-2522™). The cytotoxicity of the extracts obtained was evaluated using the MTT assay. The MTT assay was used for all produced dressing inserts (Construct P1, Construct Cur_P1, Construct P2, Construct Cur_P2). The MTT assay revealed that extracts from the biomaterials showed no cytotoxicity towards BJ cells, both after 24 and 48 hours of incubation (Fig. 12A and C). In the case of biomaterials enriched with curdlan (Construct Cur_P1 and Construct Cur_P2), higher cell viability was observed compared to biomaterials containing the superabsorbent only. In an earlier publication, we demonstrated that the addition of curdlan with calcium ions significantly stimulated the viability of BJ cells.[15] The results obtained in this study also indicate the beneficial effect of adding curdlan with calcium ions on BJ cell viability. Interestingly, the obtained results indicate that the type of PI used also had an impact on the viability of skin cells, as significantly higher viability was observed for the Construct Cur_P2 biomaterial, with values reaching 93.42 ± 4.2% (24 h) and 92.5 ± 6.3% (48 h). To further confirm the results obtained in the MTT assay, BJ cells cultured with extracts were visualized using live/dead staining. The obtained confocal laser scanning microscopy (CLSM) images showed that regardless of the extract used for culture, the cells exhibited normal morphology, and no dead cells were observed (red fluorescence) (Fig. 12B and D). Subsequent analysis, evaluating the effect of the obtained extracts on skin cell proliferation, confirmed the results obtained in the MTT assay to some extent. Specifically, the extract obtained from Construct Cur_P2 showed the most favorable impact on cell proliferation after 5 days of incubation. Nevertheless, none of the extracts exhibited significant inhibitory effects, which were further confirmed using CLSM (Fig. 12F). The number of cells treated with extracts was similar to that in the control (culture without extract). The impact of biomaterial extracts on the synthesis of type I collagen was also assessed (Fig. 12G). Observations using CLSM indicated that the biomaterials did not hinder the proper deposition of type I collagen in the extracellular matrix (ECM). This is a positive outcome, as dysregulated growth and excessive collagen formation can lead to the development of hypertrophic scars characterized by unfavorable cosmetic and functional changes in patients.[47]

### 3.11. Mutagenicity test

The Ames test is a widely used method for assessing the mutagenic potential of chemical substances by determining whether they can induce mutations in the DNA of bacteria. This test utilizes strains of *Salmonella typhimurium* that have been genetically modified to lack the ability to synthesize histidine. Mutagenic substances can induce mutations that restore the bacteria's ability to synthesize histidine, which is observed as colony growth on histidine-free media.

The Ames test was conducted to evaluate the potential mutagenicity of the tested wound dressing biomaterials, particularly due to the use of acrylic acid in their production. Acrylic acid is a well-known chemical compound that exhibits toxicity in its monomeric form. Although the polymerization process neutralizes the toxic properties of acrylic acid, it was essential to confirm the biological safety of the final products and demonstrate that the final materials do not induce genetic mutations, which could potentially lead to carcinogenic effects or other adverse health outcomes.

According to the Ames test procedure, the analyzed substance is considered non-mutagenic if: the total number of wells with revertants in the test strain TA100 is not more than twice as compared to the control, and the total number of wells with revertants in the test strain TA98 is not more than three times as compared to the control. Based on our Ames test for the tested biomaterials (Construct P1, Construct Cur_P1, Construct P2, Construct Cur_P2), the number of wells with revertants was comparable to the control (Table 3), so it can be stated that the tested biomaterials can be defined as non-mutagenic. The obtained result of non-mutagenicity of the generated constructs is crucial in the context of potential biomedical applications.

### 3.12. Blood compatibility tests: hemolysis and blood clot formation test

The ability to stop bleeding is crucial in the design of wound dressings, as it prevents excessive blood loss. In an experiment to assess the hemostatic properties of biomaterials (Fig. 13A), the Construct Cur P2 material exhibited the best properties among all the tested variants, with released hemoglobin levels below 0.25 mg $mL^{-1}$. The obtained values are fully consistent with those reported for high-performance hemostatic materials.[28] Compared to the positive control, this material significantly stimulated clot formation, which closely mirrors the normal blood clotting process.

The hemolysis test was another study to evaluate the safety of the biomaterials in contact with blood. The degree of hemolysis allows for assessing the risk of erythrocyte damage due to contact with the biomaterial. The results showed that the value of this parameter for all tested biomaterials did not exceed the level of the negative control, indicating that these materials are

Table 3 Results of bacterial reverse mutation test

| | TA98 | | TA100 | |
|---|---|---|---|---|
| | −S9 | +S9 | −S9 | +S9 |
| Control | 6 | 5 | 5 | 5 |
| $NaN_{3(positive\ control)}$ | — | — | 98 | 97 |
| $2\text{-}NF_{(positive\ control)}$ | 98 | 97 | — | — |
| Construct P1 | 9 | 7 | 5 | 5 |
| Construct Cur_P1 | 4 | 6 | 4 | 5 |
| Construct P2 | 5 | 9 | 4 | 4 |
| Construct Cur_P2 | 4 | 7 | 3 | 6 |

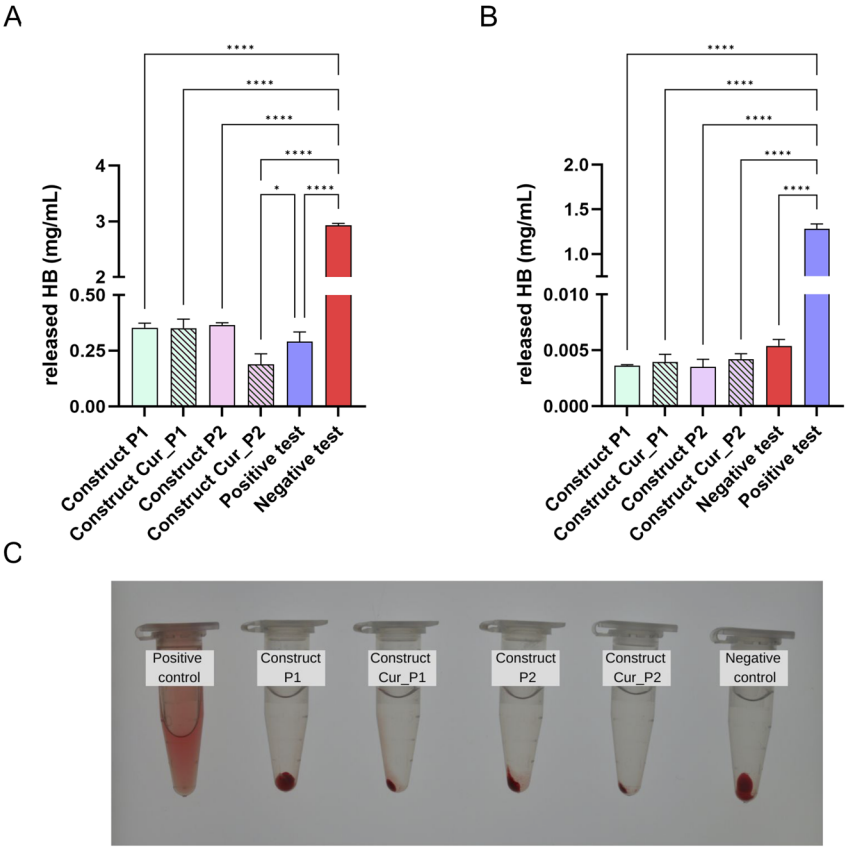


Fig. 13 (A) Quantification of clot formation induced by biomaterials. (B) Hemolysis analysis based on the concentration of released hemoglobin after incubation with biomaterials. (C) Visual comparison of hemolysis in samples incubated with the tested biomaterials, positive control, and negative control. Statistical analysis was performed using one-way ANOVA followed by Tukey's post-hoc test. Asterisks indicate statistically significant differences between the compared samples (*$p < 0.05$, ****$p < 0.0001$).

safe for applications involving contact with human blood (Fig. 13B). The results obtained in the hemolysis test are further illustrated in panel C. The positive control exhibits significant hemolysis, as evident from the intense red coloration of the sample. In contrast, all the tested biomaterials show minimal hemolysis, comparable to that of the negative control, confirming their biocompatibility.

It should be emphasized that all tested biomaterial variants demonstrated high biological safety in contact with human blood.

## 4 Conclusions

In conclusion, the results obtained in this work highlight the development of a novel 3D-printed hydrogel dressing that merges structural innovation with biological functionality. By integrating curdlan and calcium ions into a crosslinked poly(-sodium acrylate-*co*-acrylic acid)/PVP network, we created a bio-ink capable of forming soft, highly absorbent constructs that actively support biological processes relevant to wound healing rather than serving merely as passive barriers. This outstanding fluid uptake capacity, combined with a favorable water vapor transmission rate (WVTR) and effective procoagulant activity, emphasizes the superior wound-management potential of Cur_P2 compared with currently available SAP- or alginate-based systems. Beyond its technical advantages, Cur_P2 represents a new generation of dressings designed not only to absorb exudate efficiently but also to modulate the local microenvironment through controlled calcium release, supporting hemostasis and cell proliferation. Taken together, these findings demonstrate that Cur_P2 constitutes a promising platform for next-generation wound dressings that bridge material engineering and regenerative medicine, offering tangible clinical relevance and translational potential.

## Ethical statement

All experiments were performed in accordance with the guidelines of the declaration of Helsinki, and experiments were approved by the ethics committee at the Medical University of Lublin. Informed consents were obtained from human participants of this study (approval no. KE-0254/258/2020).

## Author contributions statement

The manuscript was written through the contributions of all authors. A. N.: project administration, methodology, investigation, formal analysis, software, validation, draft preparation, and writing – reviewing and editing; J. H.: methodology, investigation, formal analysis; writing L. S.: methodology,

investigation, formal analysis. B. P.: methodology, investigation, formal analysis; writing A. M.: methodology, investigation, formal analysis; writing S. T.: methodology, investigation, formal analysis; writing G. G.: project administration, supervision, draft preparation, reviewing and editing and writing – reviewing. All authors have read and agreed to the published version of the manuscript.

## Conflicts of interest

The authors declare no conflicts of interest.

## Data availability

All data supporting the findings of this study are available in the authors' own repository on Google Drive. The dataset includes all raw and processed data corresponding to the physicochemical analyses (FTIR, TGA/DTG, DSC, AFM, profilometry, wettability, ion release, WVTR, fluid absorption) as well as the results of biological experiments (cytotoxicity, proliferation, collagen synthesis, CLSM staining, Ames test, and hemocompatibility). The data can be accessed at the following link: https://drive.google.com/drive/folders/1-pdEyXxmretDmP1K2m2TWvzAVkAUXHs?usp=drive_link. We confirm that the repository contains the complete set of data underlying the results presented in this article.

## Acknowledgements

The research on compatibility with human blood was supported by the Ministry of Education and Science in Poland within the statutory activity of the Medical University of Lublin (DS6/2025). Anna Michalicha received annual support (scholarship: START) from the Foundation for Polish Science (FNP) in 2024 for the most talented young scientists. The authors sincerely thank Professor Anna Belcarz-Romaniuk from the Chair and Department of Biochemistry and Biotechnology at the Medical University of Lublin for providing the methodology for studying biomaterial interactions with human blood and her invaluable expertise. The research studies were partially conducted at Institute of High Pressure Physics using equipment funded by the Centre of Preclinical Research and Technology CePT II (RPMA.01.01.00-14-8476/17-04) and STRATEGMED3/306888/3/NCBR/2017. We would like to personally acknowledge Mr Jan Mizeracki from IHPP PAS for his technical and scientific support in SEM analyses of the samples.

## References

1 B. Cullen and A. Gefen, The Biological and Physiological Impact of the Performance of Wound Dressings, *Int. Wound J.*, 2023, 1292–1303, DOI: 10.1111/iwj.13960.
2 C. K. Sen, Human Wound and Its Burden: Updated 2020 Compendium of Estimates, *Adv. Wound Care*, 2021, **10**(5), 281–292, DOI: 10.1089/wound.2021.0026.
3 V. Falanga, R. R. Isseroff, A. M. Soulika, M. Romanelli, D. Margolis, S. Kapp, M. Granick and K. Harding, Chronic Wounds, *Nat. Rev. Dis. Primers*, 2022, **8**(50), DOI: 10.1038/s41572-022-00377-3.
4 D. Duscher, Z. N. Maan, A. J. Whittam, M. Sorkin, M. S. Hu, G. G. Walmsley, H. Baker, L. H. Fischer, M. Januszyk, V. W. Wong and G. C. Gurtner, Fibroblast-Specific Deletion of Hypoxia Inducible Factor-1 Critically Impairs Murine Cutaneous Neovascularization and Wound Healing, *Plast. Reconstr. Surg.*, 2015, **136**(5), 1004–1013, DOI: 10.1097/PRS.0000000000001699.
5 C. Wiegand and U. C. Hipler, A Superabsorbent Polymer-Containing Wound Dressing Efficiently Sequesters MMPs and Inhibits Collagenase Activity in Vitro, *J. Mater. Sci. Mater. Med.*, 2013, **24**(10), 2473–2478, DOI: 10.1007/s10856-013-4990-6.
6 J. R. Forss, Does Exudate Viscosity Affect Its Rate of Absorption into Wound Dressings?, *J. Wound Care*, 2022, **31**(3), 236–242, DOI: 10.12968/jowc.2022.31.3.236.
7 D. V. Verdolino, H. A. Thomason, A. Fotticchia, and S. Cartmell, Wound Dressings: Curbing Inflammation in Chronic Wound Healing, *Emerging Topics in Life Sciences*, Portland Press Ltd, October 1, 2021, pp. 523–537, DOI: 10.1042/ETLS20200346.
8 D. Okan, The Role of Moisture Balance in Wound Healing, *Adv. Skin Wound Care*, 2006, **20**(1), 39–53.
9 Z. Ge, W. Guo, Y. Tao, H. Sun, X. Meng, L. Cao, S. Zhang, W. Liu, M. L. Akhtar, Y. Li and Y. Ren, Wireless and Closed-Loop Smart Dressing for Exudate Management and On-Demand Treatment of Chronic Wounds, *Adv. Mater.*, 2023, **35**(47), 2304005, DOI: 10.1002/adma.202304005.
10 H. Chopra, Priyanka, O. P. Choudhary and T. B. Emran, Three Dimensional Printed Wound Dressings: Recent Progresses, *Int. J. Surg.*, 2023, **109**(3), 549–550, DOI: 10.1097/JS9.0000000000000129.
11 D. T. Uchida, and M. L. Bruschi, 3D Printing as a Technological Strategy for the Personalized Treatment of Wound Healing, *AAPS PharmSciTech*, Springer Science and Business Media Deutschland GmbH, January 1, 2023, DOI: 10.1208/s12249-023-02503-0.
12 J. Rogowska-Tylman, J. Locs, I. Salma, B. Woźniak, M. Pilmane, V. Zalite, J. Wojnarowicz, A. Kędzierska-Sar, T. Chudoba, K. Szlązak, A. Chlanda, W. Święszkowski, A. Gedanken and W. Łojkowski, *In Vivo* and *in Vitro* Study of a Novel Nanohydroxyapatite Sonocoated Scaffolds for Enhanced Bone Regeneration, *Mater. Sci. Eng. C*, 2019, **99**, 669–684, DOI: 10.1016/j.msec.2019.01.084.
13 A. G. Tabriz and D. Douroumis, Recent Advances in 3D Printing for Wound Healing: A Systematic Review, *J. Drug Deliv. Sci. Technol.*, 2022, **74**, 103564, DOI: 10.1016/j.jddst.2022.103564.
14 P. S. Gungor-Ozkerim, I. Inci, Y. S. Zhang, A. Khademhosseini, and M. R. Dokmeci, Bioinks for 3D Bioprinting: An Overview, *Biomaterials Science*, Royal Society of Chemistry, May 1, 2018, pp 915–946, DOI: 10.1039/c7bm00765e.
15 A. Nurzynska, K. Klimek, K. Palka, Ł. Szajnecki and G. Ginalska, Curdlan-Based Hydrogels for Potential Application as Dressings for Promotion of Skin Wound

Healing-Preliminary *in Vitro* Studies, *Materials*, 2021, **14**(9), 2344, DOI: 10.3390/ma14092344.

16 L. Hiendlmeier, T. F. Teshima, F. Zurita, H. Url, P. Rinklin and B. A. Wolfrum, Superabsorbent Sodium Polyacrylate Printing Resin as Actuator Material in 4D Printing, *Macromol. Mater. Eng.*, 2022, **307**(10), 2200306, DOI: 10.1002/mame.202200306.

17 N. Jahan, M. S. Ibne Mahbub, B. T. Lee and S. H. Bae, *In Vivo* and *In Vitro* Investigation of a Novel Gelatin/Sodium Polyacrylate Composite Hemostatic Sponge for Topical Bleeding, *J. Funct. Biomater.*, 2023, **14**(5), 256, DOI: 10.3390/jfb14050265.

18 Y.-D. Luo, C.-A. Dai and W.-Y. P. Chiu, AA–SA) Latex Particle Synthesis *via* Inverse Miniemulsion Polymerization–Nucleation Mechanism and Its Application in PH Buffering, *J. Colloid Interface Sci.*, 2009, **330**(1), 170–174, DOI: 10.1016/j.jcis.2008.10.036.

19 W. Wang, P. Han, L. Yang, Z. Meng, H. Gan, Z. Wu, X. Zhu, W. Sun, R. Gu and G. Dou, A Novel Sodium Polyacrylate–Based Stasis Dressing to Treat Lethal Hemorrhage in a Penetrating Trauma Swine Model, *J. Trauma Acute Care Surg.*, 2023, **94**(4), 608–614, DOI: 10.1097/TA.0000000000003869.

20 T. J. Hall, I. Azoidis, I. A. Barroso, E. A. B. Hughes, L. M. Grover and S. C. Cox, Formulation of an Antimicrobial Superabsorbent Powder That Gels *in Situ* to Produce Reactive Oxygen, *Mater. Sci. Eng. C*, 2021, **118**, 111479, DOI: 10.1016/j.msec.2020.111479.

21 T. Subramaniam, M. B. Fauzi, Y. Lokanathan and J. X. Law, The Role of Calcium in Wound Healing, *Int. J. Mol. Sci.*, 2021, **22**(12), 6486, DOI: 10.3390/ijms22126486.

22 A. Nurzyńska, G. Ginalska and Ł. Szajnecki, Method of Producing a Dressing Insert Based on Curdlan for Medical Applications, *Poland Pat.*, 445149, The Patent Office of the Republic of Poland (UPRP), 2024.

23 A. Nurzynska, K. Klimek, K. Palka, Ł. Szajnecki and G. Ginalska, Curdlan-Based Hydrogels for Potential Application as Dressings for Promotion of Skin Wound Healing-Preliminary *in Vitro* Studies, *Materials*, 2021, **14**(9), 2344, DOI: 10.3390/ma14092344.

24 S. Streich, J. Higuchi, A. Opalińska, J. Wojnarowicz, P. Giovanoli, W. Łojkowski and J. Buschmann, Ultrasonic Coating of Poly(D,L-Lactic Acid)/Poly(Lactic-Co-Glycolic Acid) Electrospun Fibers with ZnO Nanoparticles to Increase Angiogenesis in the CAM Assay, *Biomedicines*, 2024, **12**(6), 1155, DOI: 10.3390/biomedicines12061155.

25 ISO 10993-5, *Biological Evaluation of Medical Devices—Part 5: Tests for In Vitro Cytotoxicity*, International Organization for Standarization, Genewa, Switzerland, 2009.

26 S. Terpilowska and A. K. Siwicki, Interactions between Chromium(III) and Iron(III), Molybdenum(III) or Nickel(II): Cytotoxicity, Genotoxicity and Mutagenicity Studies, *Chemosphere*, 2018, **201**, 780–789, DOI: 10.1016/j.chemosphere.2018.03.062.

27 S. Terpilowska, S. Gluszek, E. Czerwosz, H. Wronka, P. Firek, J. Szmidt, M. Suchanska, J. Keczkowska, B. Kaczmarska, M. Kozlowski and R. Diduszko, Nano-Ag Particles Embedded in C-Matrix: Preparation, Properties and Application in Cell Metabolism, *Materials*, 2022, **15**(17), 5826, DOI: 10.3390/ma15175826.

28 A. Michalicha, A. Roguska, A. Przekora, B. Budzyńska and A. Belcarz, Poly(Levodopa)-Modified β-Glucan as a Candidate for Wound Dressings, *Carbohydr. Polym.*, 2021, **272**, 118485, DOI: 10.1016/j.carbpol.2021.118485.

29 F. Dai, Q. Zhuang, G. Huang, H. Deng and X. Zhang, Infrared Spectrum Characteristics and Quantification of OH Groups in Coal, *ACS Omega*, 2023, **8**(19), 17064–17076, DOI: 10.1021/acsomega.3c01336.

30 C. A. Tian and C. C. Chiu, Importance of Hydrophilic Groups on Modulating the Structural, Mechanical, and Interfacial Properties of Bilayers: A Comparative Molecular Dynamics Study of Phosphatidylcholine and Ion Pair Amphiphile Membranes, *Int. J. Mol. Sci.*, 2018, **19**(6), 1552, DOI: 10.3390/ijms19061552.

31 D. Kennepohl, S. Farmer and W. Reusch, Carboxylic acids and esters, *Org. Chem.*, 2024, **25**, 451–524.

32 C. Pagano, F. Luzi, M. Ricci, A. Di Michele, D. Puglia, M. R. Ceccarini, T. Beccari, F. Blasi, L. Cossignani, A. Schoubben, S. Primavilla, C. A. V. Iborra and L. Perioli, Wound Dressing: Combination of Acacia Gum/PVP/Cyclic Dextrin in Bioadhesive Patches Loaded with Grape Seed Extract, *Pharmaceutics*, 2022, **14**(3), 485, DOI: 10.3390/pharmaceutics14030485.

33 L. Zhang, L. Xu, J. K. Ma, Y. Y. Ye, Y. Chen and J. Y. Qian, Introduction of Curdlan Optimizes the Comprehensive Properties of Methyl Cellulose Films, *Foods*, 2023, **12**(3), 547, DOI: 10.3390/foods12030547.

34 X. Wang, J. Tang, J. Huang and M. Hui, Production and Characterization of Bacterial Cellulose Membranes with Hyaluronic Acid and Silk Sericin, *Colloids Surf. B Biointerfaces*, 2020, **195**, 111273, DOI: 10.1016/j.colsurfb.2020.111273.

35 R. Poonguzhali, S. Khaleel Basha and V. Sugantha Kumari, Novel Asymmetric Chitosan/PVP/Nanocellulose Wound Dressing: *In Vitro* and *in Vivo* Evaluation, *Int. J. Biol. Macromol.*, 2018, **112**, 1300–1309, DOI: 10.1016/j.ijbiomac.2018.02.073.

36 S. Alven, S. Peter, Z. Mbese and B. A. Aderibigbe, Polymer-Based Wound Dressing Materials Loaded with Bioactive Agents: Potential Materials for the Treatment of Diabetic Wounds, *Polymers*, 2022, **14**(4), 724, DOI: 10.3390/polym14040724.

37 M. U. A. Khan, S. Haider, M. A. Raza, S. A. Shah, S. I. A. Razak, M. R. A. Kadir, F. Subhan and A. Haider, Smart and PH-Sensitive RGO/Arabinoxylan/Chitosan Composite for Wound Dressing: In-Vitro Drug Delivery, Antibacterial Activity, and Biological Activities, *Int. J. Biol. Macromol.*, 2021, **192**, 820–831, DOI: 10.1016/j.ijbiomac.2021.10.033.

38 A. Nurzynska, K. Klimek, I. Swierzycka, K. Palka and G. Ginalska, Porous Curdlan-Based Hydrogels Modified with Copper Ions as Potential Dressings for Prevention and Management of Bacterial Wound Infection-An *in Vitro*

Assessment, *Polymers*, 2020, **12**(9), 1893, DOI: 10.3390/POLYM12091893.

39 A. Nurzynska, K. Klimek, A. Michalak, K. Dos Santos Szewczyk, M. Arczewska, U. Szalaj, M. Gagos and G. Ginalska, Do Curdlan Hydrogels Improved with Bioactive Compounds from Hop Exhibit Beneficial Properties for Skin Wound Healing?, *Int. J. Mol. Sci.*, 2023, **24**(12), 10295, DOI: 10.3390/ijms241210295.

40 G. Kammerlander, T. Eberlein and M. Algisite, *Aquacel Dressings in the Management of Various Types of Wounds*, 2003.

41 S. Hampton The Role of Alginate dressings in Wound Healing; 2004. http://www.worldwidewounds.com.

42 L. Duciel, R. Proust, A. C. Ponsen, F. Ziarelli, A. Coudreuse, L. Jeanmichel, M. Samardzic, G. Uzan and C. des. Courtils, Are All Alginate Dressings Equivalent?, *J. Biomed. Mater. Res. B Appl. Biomater.*, 2025, **113**(3), 1552, DOI: 10.1002/jbm.b.35557.

43 P. C. Masella, E. M. Balent, T. L. Carlson, K. W. Lee and L. M. Pierce, Evaluation of Six Split-Thickness Skin Graft Donor-Site Dressing Materials in a Swine Model, *Plast. Reconstr. Surg.*, 2013, **1**(9), DOI: 10.1097/GOX.0000000000000031.

44 R. Xu, H. Xia, W. He, Z. Li, J. Zhao, B. Liu, Y. Wang, Q. Lei, Y. Kong, Y. Bai, Z. Yao, R. Yan, H. Li, R. Zhan, S. Yang, G. Luo and J. Wu, Controlled Water Vapor Transmission Rate Promotes Wound-Healing *via* Wound Re-Epithelialization and Contraction Enhancement, *Sci. Rep.*, 2016, **6**, 24596, DOI: 10.1038/srep24596.

45 R. Xu, H. Xia, W. He, Z. Li, J. Zhao, B. Liu, Y. Wang, Q. Lei, Y. Kong, Y. Bai, Z. Yao, R. Yan, H. Li, R. Zhan, S. Yang, G. Luo and J. Wu, Controlled Water Vapor Transmission Rate Promotes Wound-Healing *via* Wound Re-Epithelialization and Contraction Enhancement, *Sci. Rep.*, 2016, **6**, 24596, DOI: 10.1038/srep24596.

46 C. Geri, R. Zimmer, M. Vestergaard, A. Pegalajar-Jurado and J. Hansen, From Passive to Active: Next-Generation Mechanically Active Dressings for Wound Healing, *J. Wound Care*, 2025, **34**, 9–16, DOI: 10.12968/jowc.2024.0276.

47 S. F. Ekstein, S. P. Wyles, S. L. Moran and A. Meves, Keloids: A Review of Therapeutic Management, *Int. J. Dermatol.*, 2021, 661–671, DOI: 10.1111/ijd.15159.